Balanced coupling in electromagnetic circuits

Daniel Sank ,* Mostafa Khezri, Sergei Isakov, and Juan Atalaya
Google Quantum AI, Goleta, California 93111, USA

(Received 31 May 2024; revised 4 November 2024; accepted 23 December 2024; published 5 February 2025)

The rotating-wave approximation (RWA) is ubiquitous in the analysis of driven and coupled resonators. However, the limitations of the RWA seem to be poorly understood and in some cases the RWA disposes of essential physics. We investigate the RWA in the context of electrical circuits. Using a classical Hamiltonian approach, we find that by balancing electrical and magnetic components of the resonator drive or resonator-resonator coupling, the RWA can be made exact. This type of balance, in which the RWA is exact, has applications in superconducting qubits, where it suppresses nutation normally associated with strong Rabi driving. In the context of dispersive readout, balancing the qubit-resonator coupling changes the qubit leakage induced by the resonator drive but does not remove it in the case of the transmon qubit.

DOI: 10.1103/PhysRevApplied.23.024012

I. INTRODUCTION

Analysis of driven and coupled resonators is pervasive throughout physics and engineering and the case of electrical resonators has attracted particularly strong attention due to the success of superconducting circuits in quantum computing [1,2]. Theoretical analyses almost universally use the rotating-wave approximation (RWA), wherein fast terms in the equations of motion of the system are neglected. The RWA is also invoked in the coupled-mode theory at the foundation of design of parametrically driven and nonreciprocal devices, used in, e.g., Refs. [3–5]. Each of these references ultimately refers to Ref. [6], which justifies the RWA by the fact that the RWA leads to a good approximation for the normal-mode frequencies of coupled resonators.

But how well does the RWA capture the dynamics of real devices? The RWA is known to fail in the case of superconducting qubit readout, where a weakly anharmonic resonator (transmon qubit) is coupled to a harmonic resonator. In that case, higher-order transitions between quantum levels in the coupled qubit-resonator system have been found to spoil the readout process [7], even though those transitions are absent in the traditional RWA analysis [8–11]. The RWA has also come under some scrutiny recently [12] as lowering the frequency of superconducting qubits has been pursued as a way to increase their energy-decay lifetimes. As the qubit frequency approaches the frequency of driven Rabi oscillations used for logic gates, the assumptions of the RWA are violated and it cannot be expected to be accurate. With these examples in mind, a natural question is whether we can engineer the driving or coupling of electromagnetic resonators to actually remove the fast terms at the hardware level, i.e., to make the RWA exact. If we can do this, then not only would the devices be easier to analyze but also the deleterious processes found in Ref. [7] might be suppressed.

In this paper, we show that by balancing the electric and magnetic aspects of driven and coupled resonators, we can remove the fast oscillating terms and make the RWA exact. The paper is organized as follows. In Sec. II, we provide mathematical analysis of a driven resonator, showing how proper balance between the amplitudes and phases of simultaneous capacitive (electric) and inductive (magnetic) drives makes the RWA exact. In Sec. III, we analyze two coupled resonators, showing that the RWA can be made exact if the coupling uses a balance of capacitive and inductive parts. Application to readout of superconducting qubits is discussed. In Sec. IV, we show that the RWA appears in the analysis of coupled transmission lines and that the design of a directional coupler is equivalent to making the RWA exact. Finally, we offer conclusions in Sec. V.

II. BALANCED DRIVE

A. Hamiltonian

An LC resonator driven both capacitively and inductively is shown in Fig. 1. Kirchhoff's laws for this circuit

*Contact author: sank.daniel@gmail.com

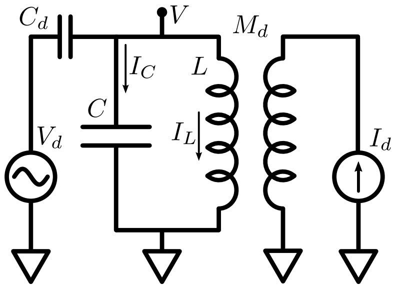

FIG. 1. The capacitively and inductively driven resonator.

are

$$C_d\left(\ddot{V}_d - \ddot{V}\right) = \dot{I}_C + \dot{I}_L, \tag{1}$$
$$L\dot{I}_L + M_d\dot{I}_d = V. \tag{2}$$

These equations lead to the Hamiltonian [13–15]

$$H = \underbrace{\frac{Q^2}{2C'} + \frac{\Phi^2}{2L}}_{H_0} + \underbrace{\frac{C_d}{C'}V_d(t)Q - \frac{M_d}{L}I_d(t)\Phi}_{H_d}, \tag{3}$$

where $C' \equiv C + C_d$. Details are given in Appendix B. The symmetry between the flux and charge terms, and between the voltage and current drive terms, is brought out by defining the impedance $Z' \equiv \sqrt{L/C'}$, the flux and charge scales $\Phi_{\text{zpf}} \equiv \sqrt{\hbar Z'/2}$ and $Q_{\text{zpf}} \equiv \sqrt{\hbar/2Z'}$ [16], and the dimensionless variables $X \equiv \Phi/2\Phi_{\text{zpf}}$ and $Y \equiv Q/2Q_{\text{zpf}}$. Using these variables, the Hamiltonian is

$$H = \underbrace{\hbar\omega_0(X^2+Y^2)}_{H_0} + \underbrace{2\,G_y y(t)Y - 2G_x x(t)X}_{H_d}, \tag{4}$$

where

$$G_x \equiv (M_d/L)\Phi_{\text{zpf}}I_d, \quad G_y \equiv (C_d/C')Q_{\text{zpf}}V_d, \tag{5}$$

and

$$I_d(t) = I_d\,x(t), \quad V_d(t) = V_d\,y(t)$$

renormalize the drive magnitudes. Here, V_d and I_d are arbitrary constants with dimensions of voltage and current, introduced so that $x(t)$ and $y(t)$ are dimensionless. The equations of motion are

$$\dot{X} = \frac{1}{2\hbar}\frac{\partial H}{\partial Y}, \quad \dot{Y} = -\frac{1}{2\hbar}\frac{\partial H}{\partial X}, \tag{6}$$

and in the absence of the drive, the solutions are $X(t) = X(0)\cos(\omega_0 t)$ and $Y(t) = -Y(0)\sin(\omega_0 t)$, where $\omega_0 = 1/\sqrt{\text{LC}'}$. This motion is analogous to a spin precessing in space as described in Appendix A and, just as is done in analysis of a driven precessing spin, it is convenient here to use a coordinate frame rotating with the intrinsic motion. Passage to the rotating coordinate frame is easier with the mode variables a and a^*, defined by

$$X = (a + a^*)/2, \quad Y = -i(a - a^*)/2.$$

With these variables, the Hamiltonian is

$$H = \underbrace{\hbar\omega_0\,|a|^2}_{H_0}\underbrace{-z(t)a - z(t)^*a^*}_{H_d}, \tag{7}$$

where $z(t) \equiv G_x\,x(t) + iG_y\,y(t)$. We switch to the rotating frame by defining $\bar{a}(t) \equiv a(t)\exp(i\omega_f\,t)$ and the Hamiltonian in the rotating frame is

$$\bar{H} = \underbrace{\hbar(\omega_0 - \omega_f)\,|\bar{a}|^2}_{\bar{H}_0}\underbrace{-z(t)\bar{a}e^{-i\omega_f\,t} - z(t)^*\bar{a}^*e^{i\omega_f\,t}}_{\bar{H}_d}. \tag{8}$$

In typical experiments, either the electric or the magnetic part of the drive is present, but not both. For example, the electric part may be absent, i.e., $V_d(t) = 0$, and the magnetic part may be sinusoidal, $I_d(t) = I_d\cos(\omega_d t)$. In this case,

$$\begin{aligned}\bar{H}_d &= -G_x\cos(\omega_d t)e^{-i\omega_f\,t}\bar{a} + \text{c.c.} \\ &= -(G_x/2)\left(e^{-i(\omega_f-\omega_d)t}\bar{a} + e^{i(\omega_f-\omega_d)t}\bar{a}^* \right. \\ &\quad \left. + e^{-i(\omega_f+\omega_d)t}\bar{a} + e^{i(\omega_f+\omega_d)t}\bar{a}^*\right).\end{aligned} \tag{9}$$

Superconducting quantum devices have resonance frequencies in the approximately 5 GHz range and control pulses are typically applied close to resonance, so while the slow terms may have frequencies $(\omega_f - \omega_d)/2\pi \lesssim 10\,\text{MHz}$, the fast terms oscillate at $(\omega_f + \omega_d)/2\pi \sim 10$ GHz. The RWA drops the fast-oscillating terms, typically with the justification that, in the weak driving limit where $G_x \ll \hbar\omega_0$, such fast terms cannot significantly affect the dynamics. It should be noted, however, that recent interest in lowering the resonance frequency of quantum devices to below 1 GHz while maintaining strong driving [17–20] pushes the limits of the weak driving assumption and so non-RWA effects may come into play.

However, if both the electric and magnetic parts of the drive are included with equal magnitude and a one-quarter-cycle phase offset, i.e.,

$$\begin{aligned} G_x &= G_y \equiv G_d, \\ x(t) &= \cos(\omega_d t + \phi_d), \\ y(t) &= \sin(\omega_d t + \phi_d), \end{aligned} \tag{10}$$

then $z(t) = G_d \exp(i(\omega_d t + \phi_d))$ and the drive Hamiltonian is

$$\bar{H}_d = -G_d \left(e^{-i(\omega_f - \omega_d)t} e^{i\phi_d} \bar{a} + \text{c.c.} \right), \tag{11}$$

where the fast terms have vanished exactly. The condition in Eq. (10) says that for the RWA to be exact, the electric and magnetic drive strengths must be equal and the charge drive must lag the flux drive by one quarter of a cycle ($\pi/2$ radians), a condition we call "balanced drive." This is the first main result of the paper: true rotating drive fields can be constructed in resonators by balancing the strengths of two drives, one coupled to each of the two conjugate variables of the resonator.

B. Trajectories of driven harmonic resonator and two-level system

The equation of motion for $\bar{a}$ corresponding to Eq. (8) is

$$\dot{\bar{a}} = -\frac{i}{\hbar} \frac{\partial \bar{H}}{\partial \bar{a}^*} = -i(\omega_0 - \omega_f)\bar{a} + \frac{iz(t)^*}{\hbar} e^{i\omega_f t}. \tag{12}$$

For an unbalanced purely inductive on-resonance drive turning on at $t = 0$, i.e., $z(t) = G\cos(\omega_0 t)$ for $t \geq 0$ and $z(t) = 0$ for $t < 0$, the time evolution of the resonator field is (taking $\omega_f = \omega_0$)

$$\bar{a}(t) = \frac{iG}{2\hbar} \left(t + \frac{e^{i2\omega_0 t} - 1}{i2\omega_0} \right). \tag{13}$$

Invoking the RWA or using balanced drive with $z(t) = (G/2)\exp(-i\omega_0 t)$ results in the second term being dropped. The dynamics with $\omega_0 = (2\pi) \times 1$ and $G/\hbar = (2\pi) \times 0.1$ are shown in Fig. 2 (these quantities can be interpreted as having any particular frequency unit and the time axis in Fig. 2 should be interpreted with the corresponding time unit, e.g., megahertz and microseconds). When the drive is balanced or when we invoke the RWA while applying an unbalanced drive, the imaginary part of the oscillator increases linearly while the real part remains zero (solid blue curve). On the other hand, when the drive is not balanced and we do not invoke the RWA, the real and imaginary parts both suffer an oscillation with period $2\pi/2\omega_0$ (broken orange curve).

Balanced drive may allow strong driving of low-frequency superconducting circuits such as fluxonium, or

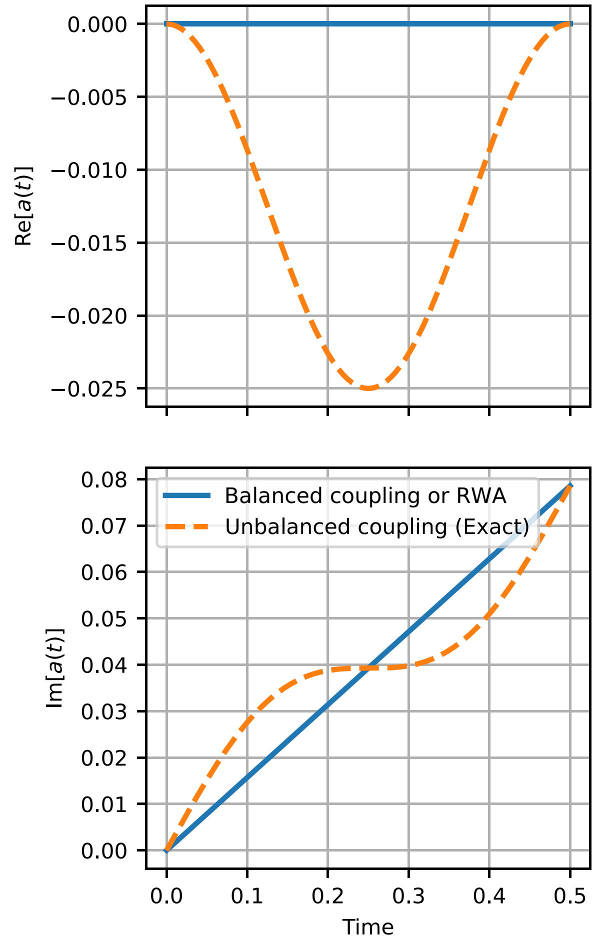

FIG. 2. The dynamics of a driven harmonic resonator. The blue solid curve corresponds to balanced drive or invoking the RWA with unbalanced drive. The orange broken curve shows the exact solution with unbalanced drive, i.e., Eq. (13).

even transmons operated at low frequency to enhance their energy-decay lifetimes T_1. The Hamiltonian for the driven two-level system may be obtained from Eq. (8) through the replacements $\bar{a} \to \sigma_-$ and $\bar{a}^* \to \sigma_+$. In Fig. 3 we show the expectation values of the Pauli operators for a two-level system driven on resonance with $\omega_0 = (2\pi) \times 1$ and $G/\hbar = (2\pi) \times 0.1$. In the exact solution with unbalanced drive (blue, green, black), the trajectory exhibits nutation, i.e., each component suffers a fast oscillation on top of the usual rotation around the Bloch sphere. On the other hand, with the balanced drive (red), the nutation is removed and the trajectories are smooth. These predictions have recently been verified in an experiment with fluxonium, where the balanced drive has been shown to remove nutation in Rabi oscillations [21]. In that experiment, the electric and magnetic drives were delivered to the qubit through two separate control lines, and the magnitudes and phases of those drives were set independently to achieve the balanced-coupling condition. One can also imagine deriving the magnetic and electric drives with only a single

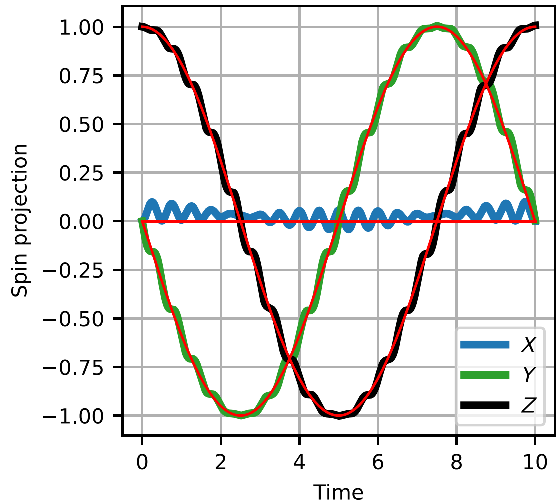

FIG. 3. The trajectory of a two-level system driven on resonance. The blue, green, and black curves show exact solutions of the X, Y, and Z projections of the system in the case of unbalanced drive. The thin red curves show the trajectories when invoking the RWA or when using balanced drive.

external source, by using that source to drive a distributed resonator and coupling the current and voltage antinodes of that resonator to the qubit. In that construction, the quarter-cycle phase shift is given automatically due to the intrinsic quarter-cycle phase lag between the current and voltage in the resonator. This approach reduces the required number of drive lines from two to one at the cost of making the drive intrinsically narrow band. However, in a fluxonium, where the range of operating frequencies is typically narrow, the limited band may be acceptable.

In electromagnetic devices where electric and magnetic couplings are commonplace, balanced drive should be realizable but we should check that the condition $G_x = G_y$ can be achieved with reasonable parameters. By inspection, G_x and G_y are proportional to the Rabi frequencies enacted by the voltage and current drives in the case of the two-level system. The Rabi frequency is related to the drive-line coupling via the equation

$$\frac{G_{x,y}}{\hbar} \propto \omega_{\text{Rabi}} = \text{constant}\sqrt{\frac{P}{\hbar Q}}, \tag{14}$$

where P is the power available in the drive line, Q is the quality factor imposed on the system due to spontaneous emission into the drive line, and the constant depends on the drive-pulse shape. The quality factor can be expressed as $Q = \omega/\Gamma$, where Γ is the spontaneous emission rate and ω is the Larmor frequency of the two-level system. So, the balanced drive condition is equivalent to

$$\frac{Q_V}{P_V} = \frac{Q_I}{P_I}, \tag{15}$$

where Q_V and Q_I are the quality factors imposed by the voltage and current drives, and P_V and P_I are the powers available on those drives.

This condition can be met in low- and high-impedance qubits. For example, for a weakly anharmonic transmon, the quality factors are approximately

$$\begin{aligned} Q_V &\approx \left(\frac{C}{C_d}\right)^2 \frac{Z}{R}, \\ Q_I &\approx \left(\frac{L}{M_d}\right)^2 \frac{R}{Z}, \end{aligned} \tag{16}$$

where L, C, and Z are the inductance, capacitance, and characteristic impedance of the transmon and R is the resistance of the transmission line carrying the drive signals. If the transmon has characteristic impedance $Z = 300\,\Omega$ and self-capacitance $C = 100\,\text{fF}$ (so that $L = 9\,\text{nH}$) and if $P_I = P_V$, then the condition is met with $M_d = 0.3\,\text{pH}$ and $C_d = 20\,\text{aF}$, which are readily realizable. In the experiment of Ref. [21], where balanced drive has been achieved in fluxonium, the target drive inductance and capacitance were 0.16 pH and 30 aF, again readily realizable [22].

III. TWO-MODE BALANCED COUPLING

A. Hamiltonian

We now consider the case of two coupled LC resonators, as shown in Fig. 4. Kirchhoff's laws for this circuit give us four equations:

$$\begin{aligned} I_{C_a} + I_{L_a} + I_g &= 0, \\ I_{C_b} + I_{L_b} - I_g &= 0, \\ L_a \dot{I}_{L_a} + L_g \dot{I}_{L_b} &= V_a, \\ L_b \dot{I}_{L_b} + L_g \dot{I}_{L_a} &= V_b. \end{aligned} \tag{17}$$

Note that the sense of the mutual inductance L_g is defined such that a positive value of $\dot{I}_{L_a}$ induces a positive contribution to V_b and vice versa. Going through the usual process of finding the Lagrangian and then converting to

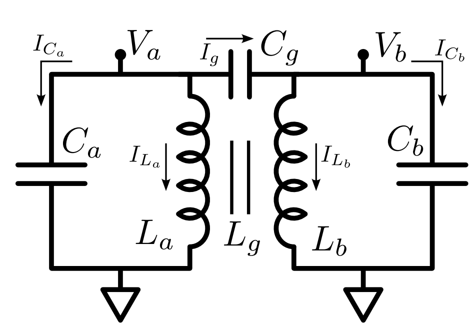

FIG. 4. Two resonators coupled capacitively and inductively.

the Hamiltonian, we find the Hamiltonian

$$H/\hbar = \omega_a' a^* a + \omega_b' b^* b \underbrace{-g_+(ab + a^*b^*) + g_-(ab^* + a^*b)}_{H_g}, \tag{18}$$

where we have defined

$$g_c \equiv \frac{1}{2}\frac{1}{C_g'\sqrt{Z_a' Z_b'}}, \quad g_l \equiv \frac{1}{2}\frac{\sqrt{Z_a' Z_b'}}{L_g'},$$
$$\text{and} \quad g_+ \equiv g_c + g_l \quad g_- \equiv g_c - g_l, \tag{19}$$

where ω', Z', C', and L' are the normalized frequency, impedance, capacitance, and inductance of the coupled resonators. Details are given in Appendix D. Evidently, there are two *aspects* to the coupling. The g_- term conserves the excitation number, while the g_+ term does not and is dropped under the RWA. Therefore, if we engineer the coupling such that g_+ is identically zero, then the RWA will be exact, i.e., the coupling Hamiltonian in the rotating frame becomes

$$\bar{H}_g/\hbar = g_-\left(\bar{a}\bar{b}^* e^{-i(\omega_a' - \omega_b')} + \text{h.c.}\right). \tag{20}$$

This observation, that a purely number-conserving interaction can be exactly realized in electromagnetic circuits, is the second main result of the paper.

The condition $g_+ = 0$ means $g_c = -g_l$, i.e., the capacitive and inductive coupling must be of equal magnitude but opposite sign, which we call "balanced coupling." Balanced coupling can also be expressed as the condition $\sqrt{-L_g'/C_g'} = \sqrt{Z_a' Z_b'}$, i.e., the coupling impedance is equal to the geometric mean of the impedances of the two resonators. Recall that a negative value for L_g means that the mutual inductance must be arranged so that a positive value of $\dot{I}_{L_a}$ produces a negative contribution to V_b. If the capacitive coupling is positive, then balanced coupling requires the mutual inductance to be negative. It should be noted that with balanced coupling, in order to achieve a certain total coupling strength g, both g_c and g_l would be *half* of what would be needed in the case of, e.g., purely capacitive coupling. Note also that strong inductive coupling has been shown even with low-impedance qubits [23].

B. Equations of motion

We take a brief aside to comment on the equations of motion arising from Eq. (18), which can be expressed in matrix form as

$$\frac{d}{dt}\begin{pmatrix} a \\ b \\ a^* \\ b^* \end{pmatrix} = -i \underbrace{\begin{pmatrix} \omega_a' & g_- & 0 & -g_+ \\ g_- & \omega_b' & -g_+ & 0 \\ 0 & g_+ & -\omega_a' & -g_- \\ g_+ & 0 & -g_- & -\omega_b' \end{pmatrix}}_{M} \begin{pmatrix} a \\ b \\ a^* \\ b^* \end{pmatrix}. \tag{21}$$

The coupling g_- connects a to b and a^* to b^*, i.e., it acts within the upper- and lower- diagonal 2×2 sub-blocks of M. On the other hand, the coupling g_+ couples a to b^* and b to a^*, as it lies on the antidiagonal of M. The structure of M and the roles of the two aspects of coupling can be clearly seen by writing M in algebraic form as

$$M = -i\left[\sigma_z \otimes \left(g_-\sigma_x + \frac{\Delta}{2}\sigma_z + \frac{S}{2}\mathbb{I}\right) - ig_+(\sigma_y \otimes \sigma_x)\right], \tag{22}$$

where $S \equiv \omega_a' + \omega_b'$ and $\Delta \equiv \omega_a' - \omega_b'$.

Dropping the g_+ terms in the Hamiltonian is equivalent to dropping the antidiagonal of M. In Appendix E, we compare the full eigenvalues of M with the eigenvalues of M under the RWA.

C. Readout

Balanced coupling may have applications in readout of superconducting qubits, which are typically measured via dispersive coupling to a harmonic resonator [8,24–26]. Unfortunately, introducing even modest levels of energy into the resonator during the readout activates resonances in the coupled qubit-resonator system that kick the qubit into noncomputational "leakage" states, i.e., those above $|0\rangle$ and $|1\rangle$ in the transmon ladder of states. This leakage is poisonous to quantum error correction [27], as occupation of noncomputational states leads to correlated errors and is difficult to reset. The physical mechanism behind leakage induced by dispersive readout was first identified in Ref. [7]. The energy levels in the joint qubit-resonator system form a Jaynes-Tavis-Cummings ladder, where the levels are coupled via excitation-preserving RWA processes and excitation-nonpreserving non-RWA processes. Considering the usual case in which the resonator frequency is larger than the qubit frequency, Ref. [11] showed that within RWA only, driving the resonator creates negligible leakage in the qubit. However, Ref. [7] showed that considering higher transmon levels above $|0\rangle$ and $|1\rangle$ and adding the non-RWA processes reveals coupling between resonant levels that causes qubit population transfer outside of the computational subspace into those higher levels. The effect was called measurement-induced state transition (MIST). The role of the transmon offset charge was pointed out in Ref. [28]. A quantitative semiclassical approach for modeling MIST was introduced in Ref. [29], together with an experimental validation of the role of transmon offset charge. Also, the semiclassical model was compared to experimental data in Ref. [29] and the authors showed that, in the unusual case in which the resonator frequency is smaller than the qubit frequency, even the RWA terms mediate MIST. Recently, the earlier results were aggregated into a unified model in Ref. [30]. MIST is a major challenge for quantum computing with superconducting qubits.

Because MIST in the usual case, in which the resonator frequency is above the qubit frequency, requires the non-RWA terms, in a circuit with balanced coupling between the qubit and resonator, MIST may be partially suppressed. Such a circuit could be implemented by direct, static, simultaneous capacitive and inductive coupling between the qubit and resonator. Alternatively, the same balancing effect could be realized in a system where the qubit-resonator coupling is purely capacitive by including an inductively coupled *drive* on the qubit to cancel the non-RWA terms, similar to the capacitive qubit driving discussed in Refs. [31,32]. On the other hand, we should not expect perfect suppression because the preceding analysis is for two coupled harmonic resonators, while qubits are by definition anharmonic. In the opposite regime, where the resonator frequency is smaller than the qubit frequency, MIST is induced mainly via RWA terms [29] and the following discussion does not apply.

To see whether or not MIST can be removed with balanced coupling, we study the matrix elements of the qubit-resonator coupling Hamiltonian between the initial qubit-resonator eigenstate $|k,n\rangle$ and either of the final states $|k+3,n-1\rangle$ or $|k+1,n+1\rangle$, which are states each having two excitations more than the initial state and therefore requiring non-RWA coupling terms. Here, k and n, respectively, label the qubit and resonator eigenstates. These particular final states are of interest because they may serve as intermediate virtual states in one of the two MIST transitions identified in Ref. [7]. The qubit-resonator coupling Hamiltonian reads as

$$H_{\text{coupling}} = \hbar\left(-g_l\Phi_{\text{q}} - ig_cQ_{\text{q}}\right)a + \hbar\left(-g_l\Phi_{\text{q}} + ig_cQ_{\text{q}}\right)a^\dagger, \tag{23}$$

where $\Phi_{\text{q}} = b + b^\dagger$ and $Q_{\text{q}} = (b - b^\dagger)/i$ are the normalized phase and charge operators of the qubit and b (a) is the bare-qubit (resonator) annihilation operator. A perturbative calculation of the coupling-matrix elements $\langle k+3, n-1|H_{\text{coupling}}|k,n\rangle$ and $\langle k+1, n+1|H_{\text{coupling}}|k,n\rangle$ is given in Appendix G and the results are shown in Fig. 5 (solid lines) along with exact numerical results (dashed lines). Interestingly, the matrix element for $|k+1,n+1\rangle$ vanishes when $g_l \approx -g_c$, similar to the balanced-coupling condition discussed above for coupled harmonic resonators. In contrast, the matrix element for $|k+3,n-1\rangle$ vanishes for $g_l = 3\,g_c$ when calculated perturbatively; however, the numerically

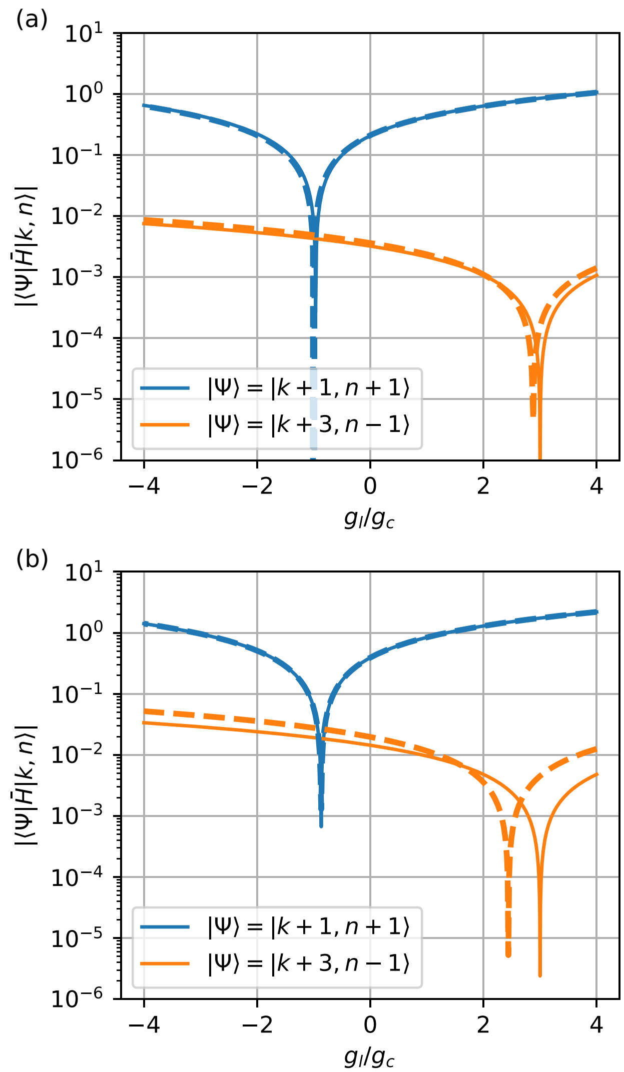

FIG. 5. The matrix elements taking the system from state $|k,n\rangle$ to $|\Psi\rangle = |k+1,n+1\rangle$ or $|k+3,n-1\rangle$. The solid lines depict the perturbative results of Appendix G and dashed lines depict the exact numerics, averaged over the offset charge: (a) $k=0$ and (b) $k=3$, which highlights that the cancellation condition depends on the value of k. Other parameters are $n=1$, $g_c/2\pi = 180$ MHz, and qubit nonlinearity coefficient $\lambda = E_C/3\sqrt{8E_JE_C} = 0.012$. Note that due to the linearity of the resonator, the matrix elements only depend on the resonator state as approximately $\sqrt{n}$; therefore, the cancellation condition does not depend on $|n\rangle$.

calculated cancellation ratio depends on the value of k, as depicted in Fig. 5. These results indicate that there is no ratio g_l/g_c for which both matrix elements vanish simultaneously, which prevents full suppression of MIST by balanced inductive and capacitive couplings.

We numerically simulate the semiclassical model described in Ref. [29] but here tailored to account for non-RWA interactions. The simulation proceeds in two steps. We first simulate the driven resonator under the influence of a classical drive, where the resonator forms a coherent state. We then treat the resonator field as a classical drive applied to the qubit [29,30]. The qubit-resonator coupling is $g = (\theta/2)\sqrt{\omega_q\omega_r}$ with coupling efficiency $\theta \approx 0.05$. The resonator frequency is $\omega_r = (2\pi)\,6\,\mathrm{GHz}$ and the resonator linewidth is $\kappa = 1/(15\,\mathrm{ns})$. The qubit frequency is set to a value between 4 GHz and 5 GHz, with transmon charging energy of $E_C = (2\pi\hbar)\,0.2\,\mathrm{GHz}$. We perform the

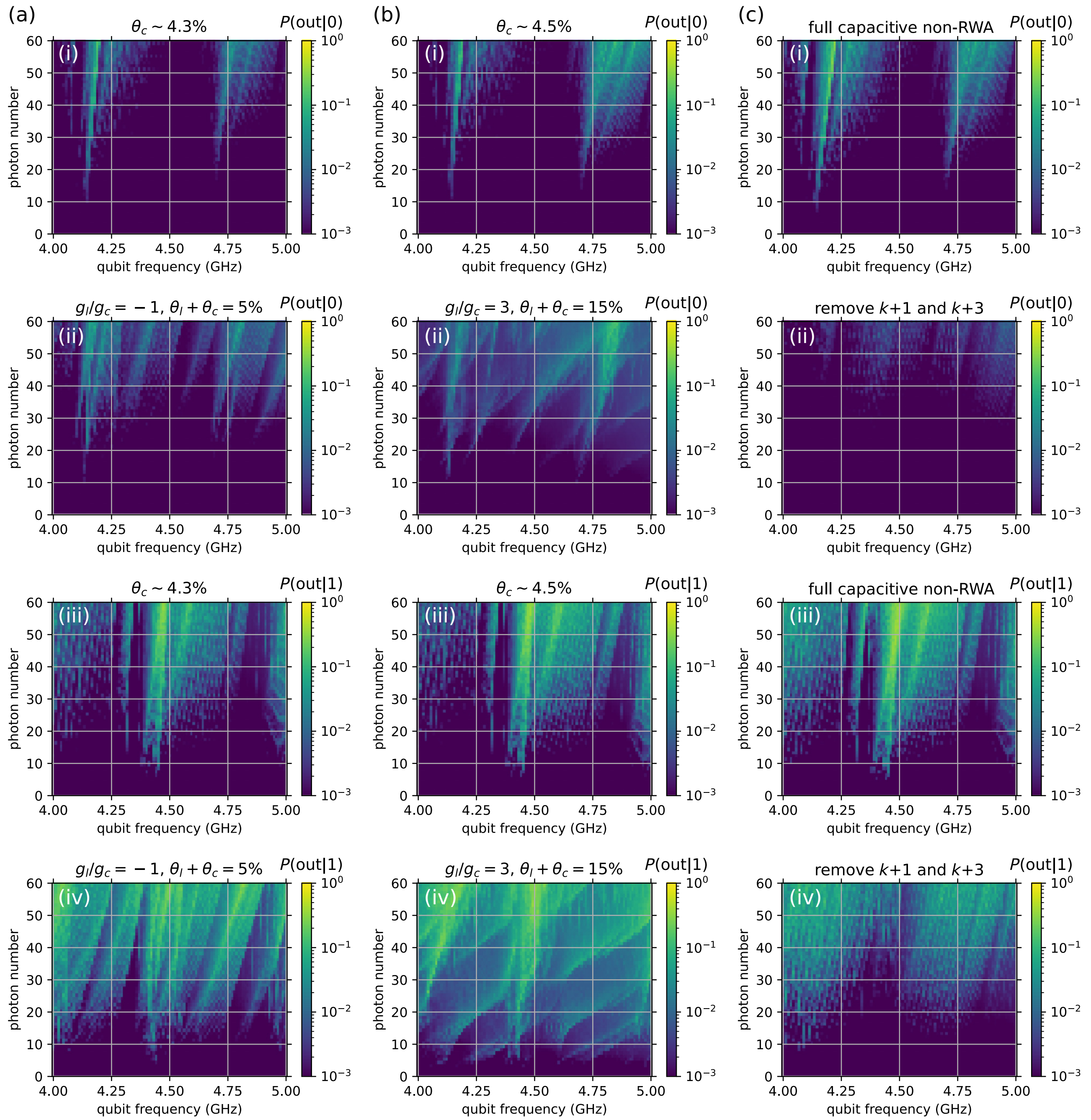

FIG. 6. Simulations of MIST for the coupled qubit-resonator with and without balanced coupling, for different g_l/g_c ratios. The first two rows show the result for a qubit prepared in $|0\rangle$ and the last two rows for a qubit prepared in $|1\rangle$. (a) Simulations for balanced coupling with $g_l/g_c = -1$, with a total balanced-coupling efficiency of 0.05: (i),(iii) the capacitive case; (ii),(iv) the balanced case. (b) Simulations with both types of couplings such that $g_l/g_c = 3$ and with a total coupling efficiency of 0.15: (i),(iii) the capacitive case; (ii),(iv) the balanced case. The large coupling efficiency is chosen to roughly yield the same dispersive shift as in the case of panels (a)(i)–(iv). (c) Simulations for the capacitive-only case with a capacitive coupling efficiency of 0.05: (i),(iii) the case in which we retain all the non-RWA terms in the Hamiltonian; (ii),(iv) the case in which we artificially remove the non-RWA corresponding to the transmon charge matrix elements $\langle k+1|Q|k\rangle$ and $\langle k+3|Q|k\rangle$ for all values of k.

simulation once with balanced coupling and a fixed total coupling efficiency and then again with purely capacitive coupling, but we adjust the latter coupling to achieve the same dispersive shift as in the balanced case at each qubit frequency. Keeping the same dispersive shift ensures a meaningful comparison of the readout performance at each frequency. We also repeat the simulation for a set of 20 equally spaced transmon gate-offset charges n_g in the range $n_g \in [-0.5, 0]$ and average the results.

The results are shown in Fig. 6. In Figs. 6(a)(i)–(a)(iv), we show the results where, for the balanced case, we take $g_l/g_c = -1$, which would cancel the non-RWA terms stemming from the $\langle k+1|Q_\mathrm{q}|k\rangle$ transmon charge matrix elements. Similarly, in Figs. 6(b)(i)–(b)(iv), we show the results where, for the balanced case, we take $g_l/g_c = 3$, which would cancel the non-RWA terms stemming from the $\langle k+3|Q_\mathrm{q}|k\rangle$ transmon charge matrix elements. Unfortunately, in both of these cases, balanced coupling does not remedy MIST and in fact makes it worse. In Figs. 6(c)(i) and 6(c)(iii), we simulate a typical case of purely capacitive coupling with all of its naturally occurring non-RWA terms and in Figs. 6(c)(ii) and 6(c)(iv), we artificially remove both of the non-RWA terms that stem from the transmon charge matrix elements mentioned above. For the initial state $|0\rangle$, we see a broad improvement. For the initial state $|1\rangle$, a large feature near qubit frequency 4.5 MHz is removed when we remove the matrix elements but the rest of the features remain more or less the same. These results suggest that besides the main two terms considered here, other non-RWA terms also play an important role in creating MIST. Note also that these results show that the balanced condition can depend on the qubit frequency and offset charge, preventing the suppression of MIST across a wide range of those parameters. Finally, while we have shown in Sec. II that the balanced drive enables smooth trajectories on the Bloch sphere under very strong Rabi oscillation in a two-level system, the findings of this section suggest that the same may not be true for a weakly harmonic device such as the transmon.

D. Antibalanced coupling

We note briefly that in the case $g_l = g_c$, the photon hopping term in the Hamiltonian in Eq. (18) vanishes and only the two-mode-squeezing terms remain. This effect has been used in Ref. [33] to engineer a nonlinear cross-Kerr interaction.

IV. COUPLED TRANSMISSION LINES

Our investigation into electromagnetic resonators with simultaneous electric and magnetic coupling was motivated by an attempt to gain intuition into why a directional coupler works. A directional coupler is a four-port microwave device that directs signal flow, as shown in Fig. 7(a). A wave injected into the top-left port is mostly transmitted through to the top-right port, while a small fraction is coupled to the lower-left port and none is coupled to the bottom-right port. The key element in a directional coupler is a pair of coupled transmission lines, which we model as an infinite ladder of lumped capacitances and inductances, as illustrated in Fig. 7(b). The coupled lines act as a directional coupler if the right-moving wave in the top line, represented by a_+ and analogous to the blue wave in Fig. 7, couples only to the left-moving wave in the bottom line, represented by b_+.

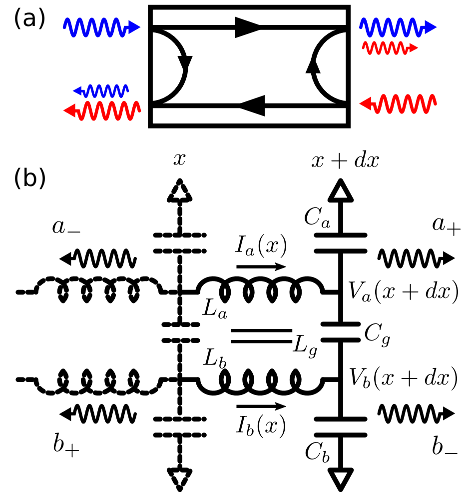

FIG. 7. (a) A directional coupler. A wave incident on the top-left port (blue) is mostly transmitted to the top-right port (large blue), while a small fraction is coupled into the bottom-left port (small blue). Similarly, a wave injected into the bottom-right port (red) is mostly transmitted to the bottom-left port (large red), while a small fraction is coupled into the top-right port (small red). (b) Capacitively and inductively coupled transmission lines. Each line is modeled as an infinite ladder of lumped capacitors and inductors. The coupling capacitance per length C_g and the coupling inductance per length L_g couple the two lines.

Line a has inductance and capacitance *per length* L_a and C_a, and similarly for line b. The lines have characteristic impedances Z_a and Z_b. The lines are coupled by a coupling inductance and capacitance per length L_g and C_g. We define amplitudes a and b by

$$\begin{aligned} a_\pm &\equiv \frac{V_a}{\sqrt{Z_a}} \pm \sqrt{Z_a} I_a, \\ b_\pm &\equiv \frac{V_b}{\sqrt{Z_b}} \mp \sqrt{Z_b} I_b. \end{aligned} \tag{24}$$

Note the similarity to the definitions of a and b in the case of coupled resonators. Assuming a sinusoidal time dependence with frequency ω, Kirchhoff's laws for the coupled-line circuit can be expressed in matrix form as

$$\frac{d}{dx}\begin{pmatrix} a_+ \\ b_+ \\ a_- \\ b_- \end{pmatrix} = i\begin{pmatrix} \beta_a & -\chi & 0 & \kappa \\ \chi & -\beta_b & -\kappa & 0 \\ 0 & -\kappa & -\beta_a & \chi \\ \kappa & 0 & -\chi & \beta_b \end{pmatrix}\begin{pmatrix} a_+ \\ b_+ \\ a_- \\ b_- \end{pmatrix}, \quad (25)$$

where $\beta = \omega/v$ is the wave vector and

$$\begin{aligned} \kappa &= \frac{\omega}{2}\left(\frac{L_g}{\sqrt{Z_a Z_b}} - C_g\sqrt{Z_a Z_b}\right) \\ \chi &= \frac{\omega}{2}\left(\frac{L_g}{\sqrt{Z_a Z_b}} + C_g\sqrt{Z_a Z_b}\right) \end{aligned} \quad (26)$$

(for details, see Appendix F). Note the resemblance between the matrix here and the matrix M that arose in the analysis of coupled resonators: each has an approximately block-diagonal form where the antidiagonal contains only a single parameter, in this case κ. Waves a_+ and b_- decouple and the lines behave as a directional coupler if $\kappa = 0$, which occurs when

$$Z_g \equiv \sqrt{\frac{L_g}{C_g}} = \sqrt{Z_a Z_b}, \quad (27)$$

i.e., when the coupling impedance is equal to the geometric mean of the characteristic impedances of the two lines, in direct analogy with the case of coupled resonators. The traveling-wave amplitudes here are analogous to the rotating-mode amplitudes in the case of coupled resonators, and the same electric-magnetic balance required to make the RWA exact in the case of coupled resonators is required to make the pair of coupled transmission lines act as a directional coupler.

The mathematical similarity of the coupled resonators and coupled transmission lines leads to an interesting insight about the design of directional couplers: because the pair of coupled transmission lines acts as a directional coupler when the RWA is exact, and as the RWA is a good approximation when the coupling is weak, a pair of coupled transmission lines will generally make a good approximation to a directional coupler, as long as the coupling is weak.

V. CONCLUSIONS

We have shown that the RWA can be made exact for both driven and coupled electromagnetic resonators. In each case, the RWA is exact when the strengths of the couplings, associated with the two conjugate degrees of freedom (flux and charge), are equal. Balancing flux and charge drives suppresses nutation in Rabi oscillations when the Rabi rate is a significant fraction of the Larmor precession frequency. While MIST is modified when the qubit-resonator coupling is balanced, there is no clear choice of electric and magnetic couplings that removes the leakage for a transmon. It may be interesting to investigate whether balanced qubit-resonator coupling can remove MIST in other superconducting qubit species.

ACKNOWLEDGMENTS

We thank Alexander Korotkov and Dvir Kafri for illuminating discussions and Andre Petukhov for encouragement.

APPENDIX A: REVIEW OF THE RWA

The phrase “rotating wave” comes from the case of a spin system driven by fields truly rotating in three-dimensional space. In the case of driven and coupled electromagnetic resonators, where geometrically rotating fields do not exist, the notion of “rotating waves” appears by mathematical analogy to the case of the spin.

Consider a magnetic moment represented by a unit vector $\vec{\rho} = (\rho_x, \rho_y, \rho_z)$. If the moment is subjected to a magnetic field $\vec{\Omega} = \gamma\vec{B} = (\Omega_x, \Omega_y, \Omega_z)$ [34], then it precesses according to

$$\frac{d}{dt}\vec{\rho} = \vec{\rho} \times \vec{\Omega}.$$

In the typical case, the magnetic field is dominated by a large static component $\vec{\Omega}_0$, which we take to lie along the z axis, $\vec{\Omega}_0 = \Omega_0\hat{z}$. In the presence of just this static field and taking $\vec{\rho}(0) = \hat{x}$, the solution is

$$\vec{\rho}(t) = \cos(\Omega_0 t)\hat{x} - \sin(\Omega_0 t)\hat{y}, \quad (A1)$$

i.e., the moment rotates clockwise about the axis of the static magnetic field with a frequency proportional to the field strength.

The moment can be visualized as a point on a sphere with coordinates θ and ϕ such that $\rho_x = \sin\theta\cos\phi$, $\rho_y = \sin\theta\sin\phi$, and $\rho_z = \cos\phi$. Suppose that we wish to control the angle θ by application of an additional drive field $\vec{\Omega}_d(t)$. In the absence of $\vec{\Omega}_0$, we could rotate $\vec{\rho}$ about the x axis with a static field oriented along $\hat{x}$; but when $\Omega_0 \neq 0$, precession about the z axis causes the relative azimuth angle between $\vec{\rho}$ and $\hat{x}$ to oscillate in time. To get a pure rotation of θ when $\Omega_0 \neq 0$, the axis of the drive field needs to rotate along with the precession induced by $\vec{\Omega}_0$, i.e.,

$$\vec{\Omega}_d(t) \propto \cos(\phi_d + \Omega_0 t)\hat{x} - \sin(\phi_d + \Omega_0 t)\hat{y}.$$

In the coordinate frame rotating with the precession induced by $\vec{\Omega}_0$, the time dependence of $\vec{\Omega}_d$ vanishes and we are left with (the subscript r indicates the rotating coordinate frame)

$$\vec{\Omega}_{d,r} \propto \cos(\phi_d)\hat{x} + \sin(\phi_d)\hat{y}, \quad (A2)$$

corresponding to a rotation about an axis in the x-y plane with azimuth angle ϕ_d.

Frequently in real-life situations, we do not have access to true rotating fields. Instead, we may have a linearly polarized field

$$\vec{\Omega}_{d,\text{linear}} \propto \cos(\Omega_0 t + \phi_d)\hat{x}.$$

The linear field can be expressed as a *pair* of rotating fields, one rotating along with the rotating frame and one rotating against the rotating frame:

$$\vec{\Omega}_{d,\text{linear}} \propto \frac{1}{2}\underbrace{\left(\cos(\Omega_0 t + \phi_d)\hat{x} - \sin(\Omega_0 t + \phi_d)\hat{y}\right)}_{\text{with frame}} + \frac{1}{2}\underbrace{\left(\cos(\Omega_0 t + \phi_d)\hat{x} + \sin(\Omega_0 t + \phi_d)\hat{y}\right)}_{\text{against frame}}.$$

In the rotating frame, these fields become

$$\vec{\Omega}_{d,\text{linear},r} \propto \frac{1}{2}\underbrace{\left(\cos(\phi_d)\hat{x} + \sin(\phi_d)\hat{y}\right)}_{\text{static}} + \frac{1}{2}\underbrace{\left(\cos(2\Omega_0 t + \phi_d)\hat{x} + \sin(2\Omega_0 t + \phi_d)\hat{y}\right)}_{\text{counterrotating}}.$$

The static part is exactly half of what we had with a true rotating field, but now there is an extra counterrotating term rotating at frequency 2Ω in the direction opposite the free precession induced by $\vec{\Omega}_0$. This inconvenient counterrotating term is precisely what is neglected in the RWA on the grounds that, because it rotates at such a high frequency, its influence on the dynamics integrates to nearly zero. When the RWA is used to drop the counterrotating term from $\vec{\Omega}_{d,\text{linear},r}$, then $\vec{\Omega}_{d,\text{linear},r} \propto \vec{\Omega}_{d,r}$. In the context of a magnetic moment suspended in space, the meaning of the term "rotating-wave approximation" is clear, as the RWA essentially replaces a linearly polarized drive field with a rotating one. With that in mind, it may seem that the use of the RWA in the context of electrical circuits, where there is no real three-dimensional space in which to construct rotating drive fields, would be inevitable. However, as shown in the main text, drives completely analogous to $\vec{\Omega}_d(t)$ can be designed in electrical circuits by proper balance of the electric and magnetic aspects of the drive.

APPENDIX B: DRIVING

1. Kirchhoff's laws

Kirchhoff's laws for the driving circuit shown in Fig. 1 are

$$\begin{aligned} C_d\left(\ddot{V}_d - \ddot{V}\right) &= \dot{I}_C + \dot{I}_L, \\ L\dot{I}_L + M_d\dot{I}_d &= V. \end{aligned} \tag{B1}$$

These two equations can be combined into a single differential equation

$$\ddot{V}\left(1 + \frac{C_d}{C}\right) + \omega_0^2 V = \frac{C_d}{C}\ddot{V}_d + \omega_0^2 M_d \dot{I}_d.$$

Defining $\Phi = \int V dt$, $C' = C + C_d$, and $\omega_0' = \omega_0/\sqrt{1 + C_d/C}$, the equation can be rewritten as

$$\ddot{\Phi} + \omega_0'^2\Phi = \frac{C_d}{C'}\dot{V}_d(t) + \omega_0'^2 M_d I_d(t). \tag{B2}$$

2. Hamiltonian form

This equation is recovered by the Lagrangian [13,14]

$$\mathcal{L} = \frac{1}{2}C\dot{\Phi}^2 - \frac{1}{2L}\Phi^2 + \frac{1}{2}C_d\left(\dot{\Phi} - V_d(t)\right)^2 + \frac{M_d}{L}I_d(t)\Phi. \tag{B3}$$

The momentum conjugate to Φ is

$$\frac{\partial\mathcal{L}}{\partial\dot{\Phi}} = C'\dot{\Phi} - C_d V_d(t) \equiv Q \tag{B4}$$

and the Hamiltonian is

$$H = Q\dot{\Phi} - \mathcal{L} \tag{B5}$$

$$= \frac{Q^2}{2C'} + \frac{\Phi^2}{2L} + \frac{C_d}{C'}V_d(t)Q - \frac{M_d}{L}I_d(t)\Phi, \tag{B6}$$

which is where we begin the analysis in the main text.

APPENDIX C: TWO-LEVEL SYSTEM

The analysis in the main text is entirely classical, with $\hbar$ an arbitrary constant with dimensions of action. However, an important case is when the driven resonator is both anharmonic and quantum mechanical, such as with superconducting qubits. If the drive frequency is set on or near resonance for only a single quantum transition $|n\rangle \to |m\rangle$, then the projection of H_d [see Eq. (3)] onto the two-level subspace spanned by those two states is approximately [35]

$$\begin{aligned} H_d &= \frac{C_d}{C_\Sigma}V_d(t)\left|Q_{n,m}\right|\sigma_y - \frac{L_d}{L}I_d(t)\left|\Phi_{n,m}\right|\sigma_x \\ &= -z(t)\sigma_- - z(t)^*\sigma_+. \end{aligned} \tag{C1}$$

where $Q_{n,m} = \langle n|Q|m\rangle$, $\Phi_{n,m} = \langle n|\Phi|m\rangle$, and $z(t)$ has the same meaning as before except that now

$$\begin{aligned} G_x &= (L_d/L)\left|\Phi_{n,m}\right| I_d, \\ G_y &= (C_d/C_\Sigma)\left|Q_{n,m}\right| V_d. \end{aligned}$$

With the drive $z(t) = G_d \exp(i(\omega_d t + \phi_d)$ and in the frame rotating at frequency ω_d,

$$\begin{aligned} H_{d,r} &= -G_d \left(e^{-i\phi_d}\sigma_+ + e^{i\phi_d}\sigma_-\right) \\ &= -G_d \begin{pmatrix} 0 & e^{i\phi_d} \\ e^{-i\phi_d} & 0 \end{pmatrix} \\ &= -G_d \left(\cos(\phi_d)\sigma_x - \sin(\phi_d)\sigma_y\right), \end{aligned} \tag{C2}$$

which is completely analogous to Eq. (A2) This result has a simple and well-known interpretation: a two-level quantum system acts like a magnetic moment (a point on the Bloch sphere) and in the rotating frame, a drive resonant with the transition of that two-level system acts like two perpendicular components of a fictitious three-dimensional drive field in the x-y plane.

APPENDIX D: COUPLING

1. Kirchhoff's laws

In order to get useful equations of motion from Kirchhoff's laws, we need to work with all voltages or all currents. We will use voltages. The capacitor currents are easily related to voltage via the constitutive equation for a capacitor: $C_i \dot{V}_i = I_i$. Note that for the coupling capacitor, the constitutive relation gives $I_g = C_g(\dot{V}_a - \dot{V}_b)$. Relating the inductor currents to voltages requires more work. The bottom two of the equations from Kirchhoff's laws can be written in matrix form as

$$\begin{pmatrix} V_a \\ V_b \end{pmatrix} = \underbrace{\begin{pmatrix} L_a & L_g \\ L_g & L_b \end{pmatrix}}_{T_L} \begin{pmatrix} \dot{I}_a \\ \dot{I}_b \end{pmatrix}.$$

The inverse of T_L is

$$\begin{aligned} T_L^{-1} &= \frac{1}{L_a L_b - L_g^2} \begin{pmatrix} L_b & -L_g \\ -L_g & L_a \end{pmatrix} \\ &\equiv \begin{pmatrix} 1/L_a' & -1/L_g' \\ -1/L_g' & 1/L_b' \end{pmatrix}, \end{aligned}$$

so that

$$\begin{aligned} \dot{I}_{L_a} &= \frac{V_a}{L_a'} - \frac{V_b}{L_g'}, \\ \dot{I}_{L_b} &= \frac{V_b}{L_b'} - \frac{V_a}{L_g'}. \end{aligned}$$

Note that

$$L_a' \equiv L_a - \frac{L_g^2}{L_b} \quad \text{and} \quad L_b' \equiv L_b - \frac{L_g^2}{L_a}$$

are the inductances to ground for each resonator, including the inductance through the mutual. Now we can rewrite all of the currents in the first two of Kirchhoff's laws entirely in terms of V_a and V_b:

$$\begin{aligned} C_a \ddot{V}_a + \frac{V_a}{L_a'} - \frac{V_b}{L_g'} + C_g(\ddot{V}_a - \ddot{V}_b) = 0 \\ C_b \ddot{V}_b + \frac{V_b}{L_b'} - \frac{V_a}{L_g'} + C_g(\ddot{V}_b - \ddot{V}_a) = 0. \end{aligned}$$

Traditional analysis of circuits in the physics literature uses flux and charge instead of current and voltage, so defining $\Phi = \int V\,dt$, we can write our equations of motion as

$$\begin{aligned} \ddot{\Phi}_a(C_a + C_g) - C_g\ddot{\Phi}_b + \frac{\Phi_a}{L_a'} - \frac{\Phi_b}{L_g'} = 0, \\ \ddot{\Phi}_b(C_b + C_g) - C_g\ddot{\Phi}_a + \frac{\Phi_b}{L_b'} - \frac{\Phi_a}{L_g'} = 0. \end{aligned} \tag{D1}$$

2. Hamiltonian form

By inspection and a bit of fiddling around, one can check that Eqs. (D1) are generated by the Lagrangian

$$\begin{aligned} \mathcal{L} = &\underbrace{\frac{C_g}{2}\left(\dot{\Phi}_a - \dot{\Phi}_b\right)^2 + \frac{C_a}{2}\dot{\Phi}_a^2 + \frac{C_b}{2}\dot{\Phi}_b^2}_{\text{kinetic}} \\ &\underbrace{-\frac{\Phi_a^2}{2L_a'} - \frac{\Phi_b^2}{2L_b'} + \frac{\Phi_a\Phi_b}{L_g'}}_{\text{potential}}. \end{aligned} \tag{D2}$$

The canonical momenta conjugate to Φ_a and Φ_b are

$$\begin{aligned} Q_a &\equiv \frac{\partial\mathcal{L}}{\partial\dot{\Phi}_a} = (C_a + C_g)\dot{\Phi}_a - C_g\dot{\Phi}_b, \\ Q_b &\equiv \frac{\partial\mathcal{L}}{\partial\dot{\Phi}_b} = (C_b + C_g)\dot{\Phi}_b - C_g\dot{\Phi}_a, \end{aligned}$$

or, in matrix form,

$$\begin{pmatrix} Q_a \\ Q_b \end{pmatrix} = \underbrace{\begin{pmatrix} (C_a + C_g) & -C_g \\ -C_g & (C_b + C_g) \end{pmatrix}}_{T_C} \begin{pmatrix} \dot{\Phi}_a \\ \dot{\Phi}_b \end{pmatrix}.$$

The matrix T_C is just the capacitance matrix of the circuit. Its inverse is

$$\begin{aligned} T_C^{-1} &= \frac{1}{C_a C_b + C_g(C_a + C_b)} \begin{pmatrix} (C_b + C_g) & C_g \\ C_g & (C_a + C_g) \end{pmatrix} \\ &\equiv \begin{pmatrix} 1/C_a' & 1/C_g' \\ 1/C_g' & 1/C_b' \end{pmatrix}. \end{aligned}$$

Note that C_a' and C_b' are simply the total capacitances to ground for each resonator.

The Hamiltonian function H for the system is defined formally by the equation

$$H \equiv \left(\sum_{i=\{a,b\}} Q_i \dot{\Phi}_i \right) - \mathcal{L},$$

where the Φ_i are the coordinates and the Q_i are the conjugate momenta, but where we have to replace the $\dot{\Phi}$'s in both the $Q\dot{\Phi}$ terms and in $\mathcal{L}$ with Φ's and Q's. To do this, first note that the kinetic term in the Lagrangian can be expressed as [36]

$$\begin{aligned}\mathcal{L}_{\text{kinetic}} &= \frac{1}{2}\langle \dot{\Phi}|T_C|\dot{\Phi}\rangle \\ &= \frac{1}{2}\langle T_C^{-1}Q|T_C|T_C^{-1}Q\rangle \\ &= \frac{1}{2}\langle Q|T_C^{-1}|Q\rangle.\end{aligned}$$

Note also that $\sum_i \dot{\Phi}_i Q_i = \langle Q|T_C^{-1}|Q\rangle$, so we can write the Hamiltonian as

$$\begin{aligned}H &= \left(\sum_{i=\{a,b\}} Q_i \dot{\Phi}_i \right) - \mathcal{L} \\ &= \langle Q|T_C^{-1}|Q\rangle - \left(\mathcal{L}_{\text{kinetic}} + \mathcal{L}_{\text{potential}}\right) \\ &= \langle Q|T_C^{-1}|Q\rangle - \left(\frac{1}{2}\langle Q|T_C^{-1}|Q\rangle + \mathcal{L}_{\text{potential}}\right) \\ &= \frac{Q_a^2}{2C_a'} + \frac{Q_b^2}{2C_b'} + \frac{\Phi_a^2}{2L_a'} + \frac{\Phi_b^2}{2L_b'} \\ &\quad + \underbrace{\frac{Q_a Q_b}{C_g'} - \frac{\Phi_a \Phi_b}{L_g'}}_{\text{coupling Hamiltonian } H_g}.\end{aligned} \tag{D3}$$

3. Dimensionless variables

We will now simplify this Hamiltonian so that we can easily find its normal modes. First, we define

$$\begin{aligned}X_i &\equiv \frac{1}{\sqrt{2\hbar}} \frac{1}{\sqrt{Z_i'}} \Phi_i, \\ Y_i &\equiv \frac{1}{\sqrt{2\hbar}} \sqrt{Z_i'} Q_i\end{aligned}$$

where $Z_i' \equiv \sqrt{L_i'/C_i'}$, and we have added the constant $\hbar$ with dimensions of action to make X and Y dimensionless. This entire analysis has been classical and in the classical case $\hbar$ can be thought of as *anything* with dimensions of action. Of course, in the quantum case, we should simply think of Φ, Q, X, and Y as operators and $\hbar$ as Planck's constant.

In the new coordinates, the Hamiltonian is

$$\begin{aligned}H/\hbar &= \omega_a' \left(X_a^2 + Y_a^2\right) + \omega_b' \left(X_b^2 + Y_b^2\right) \\ &\quad + 2\frac{1}{C_g'\sqrt{Z_a' Z_b'}} Y_a Y_b - 2\frac{\sqrt{Z_a Z_b}}{L_g'} X_a X_b,\end{aligned} \tag{D4}$$

where the $\omega_i' \equiv 1/\sqrt{L_i' C_i'}$ are called *partial frequencies* and play an important role in the analysis of the system, particularly when making approximations.

4. Rotating modes

Finally, we define

$$\begin{aligned}a &\equiv X_a + iY_a, \\ b &\equiv X_b + iY_b\end{aligned} \tag{D5}$$

to arrive at

$$\begin{aligned}H/\hbar &= \omega_a' a^* a + \omega_b' b^* b \\ &\quad - \frac{1}{2}\frac{1}{C_g'\sqrt{Z_a' Z_b'}}(ab + a^* b^* - ab^* - a^* b) \\ &\quad - \frac{1}{2}\frac{\sqrt{Z_a' Z_b'}}{L_g'}(ab + a^* b^* + a^* b + ab^*).\end{aligned} \tag{D6}$$

The stars indicate Hermitian conjugation, which in the classical case reduces to complex conjugation. The coupling term can be reorganized into the form

$$\begin{aligned}H_g/\hbar &= -\left(ab + a^* b^*\right)\frac{1}{2}\left(\frac{1}{C_g'\sqrt{Z_a' Z_b'}} + \frac{\sqrt{Z_a' Z_b'}}{L_g'}\right) \\ &\quad + \left(ab^* + a^* b\right)\frac{1}{2}\left(\frac{1}{C_g'\sqrt{Z_a' Z_b'}} - \frac{\sqrt{Z_a' Z_b'}}{L_g'}\right) \\ &= -g_+(ab + a^* b^*) + g_-(ab^* + a^* b),\end{aligned} \tag{D7}$$

where we have defined

$$\begin{aligned}&g_c \equiv \frac{1}{2}\frac{1}{C_g'\sqrt{Z_a' Z_b'}}, \quad g_l \equiv \frac{1}{2}\frac{\sqrt{Z_a' Z_b'}}{L_g'}, \\ &\text{and} \qquad g_+ \equiv g_c + g_l \quad g_- \equiv g_c - g_l,\end{aligned} \tag{D8}$$

which is the starting point in the main text.

APPENDIX E: EIGENVALUES

1. Eigenvalues in the rotating-wave approximation

The RWA provides a convenient approximation for the normal-mode frequencies of the coupled-resonator system,

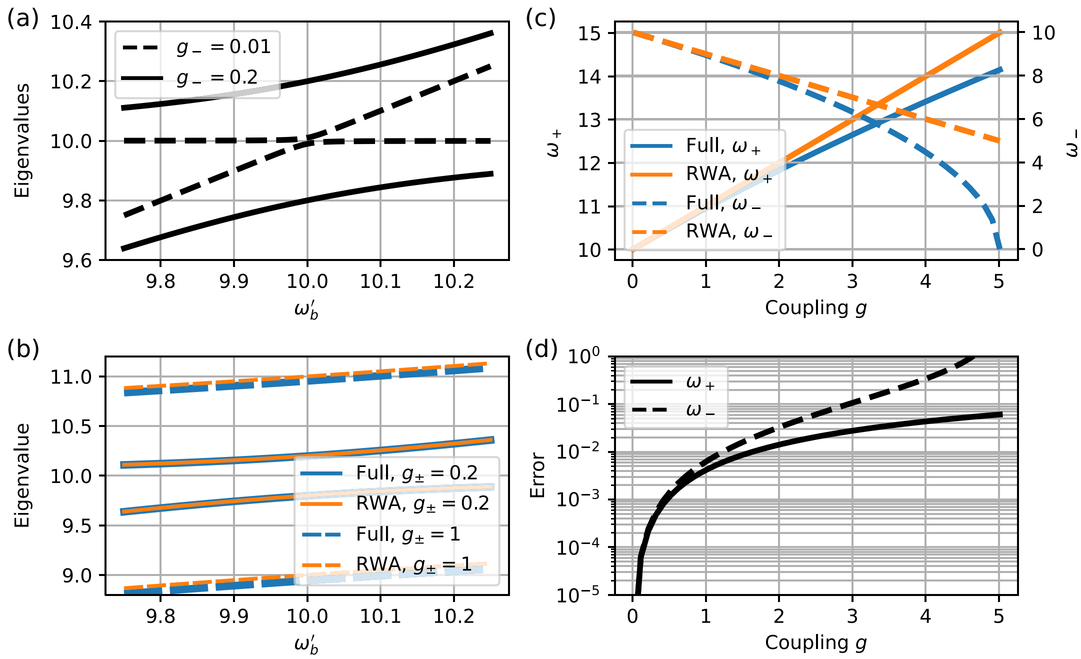

FIG. 8. The eigenvalues of the coupled-resonator system with $\omega_a' = 10$. (a) The eigenvalues $\omega_\pm$ from Eq. (E2) as a function of ω_b' for $\omega_a' = 10$. (b) The full eigenvalues (i.e., not taking the RWA) compared with the RWA. Here, g_- and g_+ are equal ($g_- = g_+ = g_\pm$), as is appropriate for resonators coupled through only one of their conjugate variables, i.e., either flux or charge. (c) The full and RWA eigenvalues $\omega_\pm$ at the avoided level crossing defined by $\omega_b' = \omega_a'$. (d) The relative error from (c).

given by the eigenvalues of M (defined in Sec. III B). In the RWA, the algebraic representation of M reduces to

$$M_{\mathrm{RWA}} = -i\sigma_z \otimes \left(g_-\sigma_x + \frac{\Delta}{2}\sigma_z + \frac{S}{2}\mathbb{I} \right). \tag{E1}$$

Equation (E1) makes finding the eigenvalues particularly simple, because the eigenvalues of a tensor product are the products of the eigenvalues of the individual factors. The eigenvalues of the quantity in parentheses, and therefore the normal-mode frequencies, are

$$\pm\omega_\pm = \pm \left(\frac{\omega_a' + \omega_b'}{2} \pm \sqrt{g_-^2 + (\Delta/2)^2} \right). \tag{E2}$$

These eigenvalues are shown in Fig. 8(a) as a function of both g_- and ω_b', where we see the famous avoided level crossing. The symmetry of Fig. 8(a) exists because we plot the normal frequencies against the frequency ω_b' rather than the uncoupled frequency ω_b.

2. Accuracy of the rotating-wave approximation

How accurate are the RWA eigenvalues plotted in Fig. 8(a)? In Fig. 8(b), we compare the full coupled-resonator eigenvalues against the RWA, working in the case that either g_c or g_l is zero, so that $g_+ = g_- \equiv g_\pm$. For $g = 0.2$, the curves are visually indistinguishable. For $g = 1$, the curves just begin to separate. In Fig, 8(c), we show the eigenvalues taken at the avoided level crossing ($\omega_b' = \omega_a'$) and in Fig. 8(d) we show the relative error of the RWA at the avoided level crossing.

APPENDIX F: COUPLED TRANSMISSION LINES

Kirchhoff's laws for the circuit shown in Fig. 7(b) are

$$\begin{aligned} V_a(x) - V_a(x+dx) &= L_a\dot{I}_a + L_g\dot{I}_b, \\ I_a(x) - I_a(x+dx) &= \dot{V}_a C_a + \left(\dot{V}_a - \dot{V}_b\right) C_g, \\ V_b(x) - V_b(x+dx) &= L_b\dot{I}_b + L_g\dot{I}_a, \\ I_b(x) - I_b(x+dx) &= \dot{V}_b C_b + \left(\dot{V}_b - \dot{V}_a\right) C_g. \end{aligned}$$

In the limit $dx \to 0$, these equations become differential equations:

$$\begin{aligned} -\frac{\partial V_a}{\partial x} &= \frac{\partial}{\partial t}\left(L_a I_a + L_g I_b\right), \\ -\frac{\partial I_a}{\partial x} &= \frac{\partial}{\partial t}\left((C_a + C_g)V_a - C_g V_b\right), \\ -\frac{\partial V_b}{\partial x} &= \frac{\partial}{\partial t}\left(L_b I_b + L_g I_a\right), \\ -\frac{\partial I_b}{\partial x} &= \frac{\partial}{\partial t}\left((C_b + C_g)V_b - C_g V_a\right). \end{aligned} \tag{F1}$$

Assuming sinusoidal time dependence at frequency ω and therefore converting time derivatives to $-i\omega$, these equations can be written in matrix form as [37]

$$\frac{d}{dx}\begin{pmatrix} V_a \\ I_a \\ V_b \\ I_b \end{pmatrix} = i\omega \begin{pmatrix} 0 & L_a & 0 & L_g \\ C_a & 0 & -C_g & 0 \\ 0 & L_g & 0 & L_b \\ -C_g & 0 & C_b & 0 \end{pmatrix} \begin{pmatrix} V_a \\ I_a \\ V_b \\ I_b \end{pmatrix}. \tag{F2}$$

If we convert to the ingoing and outcoming wave amplitudes

$$\begin{aligned} a_{\pm} &\equiv \frac{V_a}{\sqrt{Z_a}} \pm \sqrt{Z_a} I_a, \\ b_{\pm} &\equiv \frac{V_b}{\sqrt{Z_b}} \mp \sqrt{Z_b} I_b, \end{aligned} \tag{F3}$$

the equations of motion take the form

$$\frac{d}{dx}\begin{pmatrix} a_+ \\ b_+ \\ a_- \\ b_- \end{pmatrix} = i \begin{pmatrix} \beta_a & -\chi & 0 & \kappa \\ \chi & -\beta_b & -\kappa & 0 \\ 0 & -\kappa & -\beta_a & \chi \\ \kappa & 0 & -\chi & \beta_b \end{pmatrix} \begin{pmatrix} a_+ \\ b_+ \\ a_- \\ b_- \end{pmatrix}, \tag{F4}$$

where $\beta \equiv \omega/v$ is the wave vector and

$$\begin{aligned} \kappa &\equiv \frac{\omega}{2}\left(\frac{L_g}{\sqrt{Z_a Z_b}} - C_g\sqrt{Z_a Z_b}\right), \\ \chi &\equiv \frac{\omega}{2}\left(\frac{L_g}{\sqrt{Z_a Z_b}} + C_g\sqrt{Z_a Z_b}\right). \end{aligned} \tag{F5}$$

APPENDIX G: BALANCED COUPLING WITH NONLINEAR OSCILLATORS

In the main text, we have shown that the non-RWA terms ab and $a^\dagger b^\dagger$ can be exactly canceled from the Hamiltonian of two coupled linear oscillators by balancing the electric and magnetic couplings. In this appendix, we analyze the case in which one of the oscillators is a transmon qubit (a weakly nonlinear oscillator), while the other resonator is the qubit readout resonator, assumed to be a linear oscillator. In contrast to the linear case, we will show that, in the nonlinear case, new non-RWA terms appear that cannot be simultaneously canceled under the balanced-coupling condition. In this appendix, we use a quantum description throughout.

We use the following approximate Hamiltonian for the transmon qubit [38]:

$$H_{\mathrm{q}} = \hbar\omega_p\left[b^\dagger b + \frac{1}{2} - \lambda\left(\frac{b+b^\dagger}{\sqrt{2}}\right)^4\right], \tag{G1}$$

where b and $b^\dagger$ are the (bare) qubit annihilation and creation operators, respectively. $\omega_p = \sqrt{8E_c E_J}/\hbar$ is the plasma frequency, where E_c and E_J are, respectively, the charging and Josephson energies. $\lambda = E_c/(3\hbar\omega_p)$ is a dimensionless parameter characterizing the strength of the qubit nonlinearity ($\lambda > 0$). Typically for a transmon qubit, λ is of order of 10^{-2}. Here, we define the dimensionless charge ($\hat{Q}_{\mathrm{q}}$) and flux ($\hat{\Phi}_{\mathrm{q}}$) operators of the qubit as

$$Q_{\mathrm{q}} = \frac{b - b^\dagger}{i}, \quad \Phi_{\mathrm{q}} = b + b^\dagger. \tag{G2}$$

These dimensionless operators are normalized differently than X and Y in the main text; in particular, here $\left[\Phi_{\mathrm{q}}, Q_{\mathrm{q}}\right] = 2i$. The qubit readout resonator is assumed to be linear, with a Hamiltonian equal to $H_{\mathrm{r}} = \hbar\omega_{\mathrm{r}} a^\dagger a$, where a and $a^\dagger$ are the photon annihilation and creation operators. The dimensionless charge and flux operators for the readout resonator are

$$Q_{\mathrm{r}} = \frac{a - a^\dagger}{i}, \quad \Phi_{\mathrm{r}} = a + a^\dagger. \tag{G3}$$

The coupling between the two oscillators is similar to the electric-magnetic coupling discussed in the main text,

$$\begin{aligned} H_{\mathrm{coupling}} &= \hbar g_c Q_{\mathrm{q}} Q_{\mathrm{r}} - \hbar g_l \Phi_{\mathrm{q}} \Phi_{\mathrm{r}} \\ &= -\hbar g_c (b - b^\dagger)(a - a^\dagger) - \hbar g_l (b + b^\dagger)(a + a^\dagger). \end{aligned} \tag{G4}$$

The balanced-coupling condition reads as $g_c = -g_l$.

The analysis of the non-RWA terms is carried out in the eigenbasis of each oscillator. We denote the eigenbasis of the transmon qubit by $|k\rangle$, where $k = 0, 1, 2, \ldots$. We can use perturbation theory to obtain the qubit eigenstates in terms of the bare-qubit states $|k\rangle_{\mathrm{bare}}$ [38] and determine the unitary operator U that relates them,

$$|k\rangle = U|k\rangle_{\mathrm{bare}}. \tag{G5}$$

To first order in λ, U is given by ($\mathbb{1}$ is the identity operator)

$$U = \mathbb{1} - \frac{\lambda}{4}\left[\frac{b^4}{4} - \frac{{b^\dagger}^4}{4} + b^2(2bb^\dagger - 3) - (2bb^\dagger - 3){b^\dagger}^2\right]. \tag{G6}$$

Using Eq. (G6), the qubit eigenstates $|k\rangle$, to first order in λ, are given by

$$\begin{aligned} |k\rangle = |k\rangle_{\mathrm{bare}} - \frac{\lambda}{4}\Bigg[& \frac{\sqrt{k(k-1)(k-2)(k-3)}}{4}\,|k-4\rangle_{\mathrm{bare}} \\ & - \frac{\sqrt{(k+1)(k+2)(k+3)(k+4)}}{4}\,|k+4\rangle_{\mathrm{bare}} \\ & + (2k-1)\sqrt{k(k-1)}\,|k-2\rangle_{\mathrm{bare}} \\ & - (2k+3)\sqrt{(k+1)(k+2)}\,|k+2\rangle_{\mathrm{bare}}\Bigg], \end{aligned} \tag{G7}$$

which coincides with Eq. (A.31) of Ref. [38].

In the qubit-eigenstate basis, the annihilation operator b transforms into the operator $\bar{b}$, which, to first order in λ, is given by

$$\bar{b} \equiv U^\dagger b U = b + \frac{\lambda}{4} b^{\dagger 3} - \frac{\lambda}{2} b^3 + \frac{3\lambda}{2}(b^\dagger b) b^\dagger. \tag{G8}$$

Equation (G8) is useful to compute the matrix elements $b_{kk'} = \langle k|b|k'\rangle$, as the latter can be rewritten

$$b_{kk'} = {}_{\mathrm{bare}}\langle k|U^\dagger b U|k'\rangle_{\mathrm{bare}} = {}_{\mathrm{bare}}\langle k|\bar{b}|k'\rangle_{\mathrm{bare}}. \tag{G9}$$

Similarly, in the qubit-eigenstate basis, the charge and flux operators are

$$\begin{aligned}\bar{\Phi}_{\mathrm{q}} &\equiv U^\dagger \Phi_{\mathrm{q}} U = \bar{b} + \bar{b}^\dagger \\ &= b + b^\dagger - \frac{\lambda}{4}\left(b^3 + b^{\dagger 3}\right) + \frac{3\lambda}{2}\left(b(b^\dagger b) + (b^\dagger b) b^\dagger\right),\end{aligned} \tag{G10}$$

$$\begin{aligned}i\bar{Q}_{\mathrm{q}} &\equiv i\, U^\dagger Q_{\mathrm{q}} U = \bar{b} - \bar{b}^\dagger \\ &= \left[b - b^\dagger - \frac{3\lambda}{4}\left(b^3 - b^{\dagger 3}\right) - \frac{3\lambda}{2}\left(b(b^\dagger b) - (b^\dagger b) b^\dagger\right)\right],\end{aligned} \tag{G11}$$

and the coupling Hamiltonian becomes

$$\begin{aligned}\bar{H}_{\mathrm{coupling}} &= U^\dagger H_{\mathrm{coupling}} U \\ &= \hbar\left(-g_l \bar{\Phi}_{\mathrm{q}} - i g_c \bar{Q}_{\mathrm{q}}\right) a + \hbar\left(-g_l \bar{\Phi}_{\mathrm{q}} + i g_c \bar{Q}_{\mathrm{q}}\right) a^\dagger.\end{aligned} \tag{G12}$$

Let us assume that the balanced-coupling condition holds, i.e., $g_c = -g_l = g/2$. After inserting Eqs. (G10)–(G11) into Eq. (G12), we find that the balanced-coupling Hamiltonian still includes non-RWA terms,

$$\bar{H}^{(\mathrm{balanced})}_{\mathrm{coupling}} = \bar{H}_{\mathrm{RWA}} + \bar{H}_{\mathrm{non}}\text{-RWA}, \tag{G13}$$

where

$$\bar{H}_{\mathrm{RWA}} = g(ab^\dagger + a^\dagger b)$$

is the desired effective RWA coupling between the eigenstates $|k,n\rangle$ and $|k \mp 1, n \pm 1\rangle$, belonging to the same RWA strip with $n_\Sigma = n + k$ excitations [38], where n indicates the number of photons in the readout resonator (an RWA strip with n_Σ excitations is defined as the subspace of states $|k,n\rangle$ such that $n + k = n_\Sigma$).

The non-RWA terms in the coupling are given by

$$\bar{H}_{\mathrm{non}}\text{-RWA} = g\lambda\left[\frac{3}{2}(b^\dagger b) b^\dagger a^\dagger - \frac{1}{2} b^{\dagger 3} a + \frac{1}{4} b^{\dagger 3} a^\dagger\right] + \text{H.c.} \tag{G14}$$

There are two types of non-RWA terms in Eq. (G14). The first type of non-RWA terms includes the terms $(b^\dagger b) b^\dagger a^\dagger$ and $b^{\dagger 3} a$ (as well as their Hermitian-conjugated terms) that couple states of two RWA strips separated by two excitations. The second type of non-RWA terms consists of $b^{\dagger 3} a^\dagger$ and its Hermitian conjugate that couple RWA strips separated by four excitations [38], which are ignored in our discussions, since those RWA strips are much further detuned and do not participate as much in the eigenenergy formation of the system. These non-RWA couplings open the way to MIST between, e.g., the qubit ground state and high-energy qubit eigenstates during qubit readout. It is not possible to find a suitable operation point (g_c, g_l) that eliminates all non-RWA terms.

More generally, we investigate the matrix elements involved in moving the system from one RWA strip to another one with two more excitations. The matrix elements of H_{coupling} involved in the transition $|k,n\rangle \to |k+1, n+1\rangle$ are

$$\begin{aligned}&\langle k+1, n+1|\Phi_{\mathrm{q}} a^\dagger|k,n\rangle \\ &\quad = \sqrt{n+1}\left(\sqrt{k+1} + \frac{3\lambda}{2}(k+1)^{3/2}\right)\end{aligned} \tag{G15}$$

and

$$\begin{aligned}&\langle k+1, n+1|iQ_{\mathrm{q}} a^\dagger|k,n\rangle \\ &\quad = \sqrt{n+1}\left(-\sqrt{k+1} + \frac{3\lambda}{2}(k+1)^{3/2}\right)\end{aligned} \tag{G16}$$

and the matrix elements in involved in the transition $|k,n\rangle \to |k+3, n-1\rangle$ are

$$\langle k+3, n-1|\Phi_{\mathrm{q}} a|k,n\rangle = -\sqrt{n}\frac{\lambda}{4}\sqrt{(k+1)(k+2)(k+3)}, \tag{G17}$$

$$\langle k+3, n-1|iQ_{\mathrm{q}} a|k,n\rangle = \sqrt{n}\frac{3\lambda}{4}\sqrt{(k+1)(k+2)(k+3)}. \tag{G18}$$

From Eqs. (G12) and (G17)–(G18), we find that (to leading order in λ) the Hamiltonian matrix element associated with the transition $|k,n\rangle \to |k+3, n-1\rangle$ can be eliminated if $g_l = 3g_c$.

[1] P. Krantz, M. Kjaergaard, F. Yan, T. P. Orlando, S. Gustavsson, and W. D. Oliver, A quantum engineer's guide to superconducting qubits, Appl. Phys. Rev. **6**, 021318 (2019).

[2] A. Blais, A. L. Grimsmo, S. M. Girvin, and A. Wallraff, Circuit quantum electrodynamics, Rev. Mod. Phys. **93**, 025005 (2021).

[3] F. Lecocq, L. Ranzani, G. Peterson, K. Cicak, R. Simmonds, J. Teufel, and J. Aumentado, Nonreciprocal microwave signal processing with a field-programmable Josephson amplifier, Phys. Rev. Appl. **7**, 024028 (2017).

[4] G. A. Peterson, F. Lecocq, K. Cicak, R. W. Simmonds, J. Aumentado, and J. D. Teufel, Demonstration of efficient nonreciprocity in a microwave optomechanical circuit, Phys. Rev. X **7**, 031001 (2017).

[5] L. Ranzani and J. Aumentado, Graph-based analysis of nonreciprocity in coupled-mode systems, New J. Phys. **17**, 023024 (2015).

[6] W. H. Louisell, *Parametric and Coupled Mode Electronics* (John Wiley & Sons, Inc., London, 1960).

[7] D. Sank *et al.*, Measurement-induced state transitions in a superconducting qubit: Beyond the rotating wave approximation, Phys. Rev. Lett. **117**, 190503 (2016).

[8] D. I. Schuster, A. Wallraff, A. Blais, L. Frunzio, R.-S. Huang, J. Majer, S. M. Girvin, and R. J. Schoelkopf, ac Stark shift and dephasing of a superconducting qubit strongly coupled to a cavity field, Phys. Rev. Lett. **94**, 123602 (2005).

[9] A. Wallraff, D. I. Schuster, A. Blais, L. Frunzio, R.-S. Huang, J. Majer, S. Kumar, S. M. Girvin, and R. J. Schoelkopf, Strong coupling of a single photon to a superconducting qubit using circuit quantum electrodynamics, Nature **431**, 162 (2004).

[10] A. Blais, R.-S. Huang, A. Wallraff, S. Girvin, and R. J. Schoelkopf, Cavity quantum electrodynamics for superconducting electrical circuits: An architecture for quantum computation, Phys. Rev. A **69**, 062320 (2004).

[11] M. Khezri, E. Mlinar, J. Dressel, and A. N. Korotkov, Measuring a transmon qubit in circuit QED: Dressed squeezed states, Phys. Rev. A **94**, 012347 (2016).

[12] D. Zeuch, F. Hassler, J. J. Slim, and D. P. DiVincenzo, Exact rotating wave approximation, Ann. Phys. **423**, 168327 (2020).

[13] U. Vool and M. Devoret, Introduction to quantum electromagnetic circuits, Int. J. Circuit Theory Appl. **45**, 897 (2017).

[14] S. M. Girvin, in *Quantum Machines: Measurement and Control of Engineered Quantum Systems: Lecture Notes of the Les Houches Summer School: Volume 96, July 2011* (Oxford University Press, Oxford, 2014).

[15] A. Ciani, D. P. DiVincenzo, and T. B. M., Lecture notes on quantum electrical circuits, (TU Delft OPEN Publishing, Delft, 2024).

[16] Φ_{zpf} and Q_{zpf} are the flux and charge zero-point fluctuations in the ground state of the quantum LC resonator.

[17] H. Zhang, S. Chakram, T. Roy, N. Earnest, Y. Lu, Z. Huang, D. Weiss, J. Koch, and D. I. Schuster, Universal fast-flux control of a coherent, low-frequency qubit, Phys. Rev. X **11**, 011010 (2021).

[18] B.-L. Najera-Santos, R. Rousseau, K. Gerashchenko, H. Patange, A. Riva, M. Villiers, T. Briant, P.-F. Cohadon, A. Heidmann, and J. Palomo *et al.*, High-sensitivity ac-charge detection with a mHz-frequency fluxonium qubit, Phys. Rev. X **14**, 011007 (2024).

[19] P. D. Kurilovich, T. Connolly, C. G. L. Bøttcher, D. K.Weiss, S. Hazra, V. R. Joshi, A. Z. Ding, H. Nho, S. Diamond, V. D. Kurilovich, W. Dai, V. Fatemi, L. Frunzio, L. I. Glazman, and M. H. Devoret, High-frequency readout free from transmon multi-excitation resonances, arXiv:2501.09161.

[20] D. L. Campbell, Y.-P. Shim, B. Kannan, R. Winik, D. K. Kim, A. Melville, B. M. Niedzielski, J. L. Yoder, C. Tahan, S. Gustavsson, and W. D. Oliver, Universal nonadiabatic control of small-gap superconducting qubits, Phys. Rev. X **10**, 041051 (2020).

[21] D. A. Rower, L. Ding, H. Zhang, M. Hays, J. An, P. M. Harrington, I. Rosen, J. M. Gertler, T. M. Hazard, B. M. Niedzielski, M. E. Schwartz, S. Gustavsson, K. Serniak, J. A. Grover, and W. D. Oliver, Suppressing counter-rotating errors for fast single-qubit gates with fluxonium, PRX Quantum **5**, 040342 (2024).

[22] Private communication. Note that we do not know the power used for the capacitive and inductive drives in Ref. [21].

[23] Y. Chen *et al.*, Qubit architecture with high coherence and fast tunable coupling, Phys. Rev. Lett. **113**, 220502 (2014).

[24] A. Wallraff, D. Schuster, A. Blais, L. Frunzio, J. Majer, M. Devoret, S. Girvin, and R. Schoelkopf, Approaching unit visibility for control of a superconducting qubit with dispersive readout, Phys. Rev. Lett. **95**, 060501 (2005).

[25] E. Jeffrey, D. Sank, J. Y. Mutus, T. C. White, J. Kelly, R. Barends, Y. Chen, Z. Chen, B. Chiaro, A. Dunsworth, A. Megrant, P. J. J. O'Malley, C. Neill, P. Roushan, A. Vainsencher, J. Wenner, A. N. Cleland, and J. M. Martinis, Fast accurate state measurement with superconducting qubits, Phys. Rev. Lett. **112**, 190504 (2014).

[26] J. Heinsoo, C. K. Andersen, A. Remm, S. Krinner, T. Walter, Y. Salathé, S. Gasparinetti, J.-C. Besse, A. Potočnik, A. Wallraff, and C. Eichler, Rapid high-fidelity multiplexed readout of superconducting qubits, Phys. Rev. Appl. **10**, 034040 (2018).

[27] K. C. Miao, M. McEwen, J. Atalaya, D. Kafri, L. P. Pryadko, A. Bengtsson, A. Opremcak, K. J. Satzinger, Z. Chen, and P. V. Klimov *et al.*, Overcoming leakage in quantum error correction, Nat. Phys. **19**, 1780 (2023).

[28] M. Malekakhlagh, W. Shanks, and H. Paik, Optimization of the resonator-induced phase gate for superconducting qubits, Phys. Rev. A **105**, 022607 (2022).

[29] M. Khezri, A. Opremcak, Z. Chen, K. C. Miao, M. McEwen, A. Bengtsson, T. White, O. Naaman, D. Sank, A. N. Korotkov, Y. Chen, and V. Smelyanskiy, Measurement-induced state transitions in a superconducting qubit: Within the rotating-wave approximation, Phys. Rev. Appl. **20**, 054008 (2023).

[30] M. F. Dumas, B. Groleau-Paré, A. McDonald, M. H. Muñoz-Arias, C. Lledó, B. D'Anjou, and A. Blais, Measurement-induced transmon ionization, Phys. Rev. X **14**, 041023 (2024).

[31] M. H. Muñoz-Arias, C. Lledó, and A. Blais, Qubit readout enabled by qubit cloaking, Phys. Rev. Appl. **20**, 054013 (2023).

[32] C. Lledó, R. Dassonneville, A. Moulinas, J. Cohen, R. Shillito, A. Bienfait, B. Huard, and A. Blais, Cloaking a qubit in a cavity, Nat. Commun. **14**, 6313 (2023).

[33] M. Kounalakis, C. Dickel, A. Bruno, N. Langford, and G. Steele, Tuneable hopping and nonlinear cross-Kerr

interactions in a high-coherence superconducting circuit, npj Quantum Inf. **4**, 38 (2018).
[34] $\vec{\Omega} = \gamma \vec{B}$ where γ is the gyromagnetic ratio, so $\vec{\Omega}$ has dimensions of frequency.
[35] This approximation leaves out terms proportional to σ_z, which can usually be ignored under assumptions similar to the RWA.
[36] Because matrix transposition and inversion commute, and because the matrix T_C is symmetric, we can bring T_C^{-1} from the bra onto the ket for free.
[37] The choice of sign in $-i\omega$ makes positive values of the wave vector correspond to right-moving waves.
[38] M. Khezri, Ph.D. thesis, University of California, Riverside, 2018.